Geomorphology 214 (2014) 324–338

Contents lists available at ScienceDirect

Geomorphology

journal homepage: www.elsevier.com/locate/geomorph

Characterizing the primary material sources and dominant erosional processes for post-fire debris-flow initiation in a headwater basin using multi-temporal terrestrial laser scanning data

Dennis M. Staley [a,*], Thad A. Wasklewicz [b], Jason W. Kean [a]

[a] U.S. Geological Survey, P.O. Box 250466, MS966 DFC, Denver, CO, USA
[b] East Carolina University, Greenville NC, USA

ARTICLE INFO

Article history:
Received 3 May 2013
Received in revised form 7 February 2014
Accepted 22 February 2014
Available online 1 March 2014

Keywords:
Wildfire
Debris flow
Geomorphic change detection
Erosion
San Gabriel Mountains
California

ABSTRACT

Wildfire dramatically alters the hydrologic response of a watershed such that even modest rainstorms can produce hazardous debris flows. Relative to shallow landslides, the primary sources of material and dominant erosional processes that contribute to post-fire debris-flow initiation are poorly constrained. Improving our understanding of how and where material is eroded from a watershed during a post-fire debris-flow requires (1) precise measurements of topographic change to calculate volumetric measurements of erosion and deposition, and (2) the identification of relevant morphometrically defined process domains to spatially constrain these measurements of erosion and deposition. In this study, we combine the morphometric analysis of a steep, small (0.01 km^2) headwater drainage basin with measurements of topographic change using high-resolution (2.5 cm) multi-temporal terrestrial laser scanning data made before and after a post-fire debris flow. The results of the morphometric analysis are used to define four process domains: hillslope-divergent, hillslope-convergent, transitional, and channelized incision. We determine that hillslope-divergent and hillslope-convergent process domains represent the primary sources of material over the period of analysis in the study basin. From these results we conclude that raindrop-impact induced erosion, ravel, surface wash, and rilling are the primary erosional processes contributing to post-fire debris-flow initiation in the small, steep headwater basin. Further work is needed to determine (1) how these results vary with increasing drainage basin size, (2) how these data might scale upward for use with coarser resolution measurements of topography, and (3) how these results change with evolving sediment supply conditions and vegetation recovery.
Published by Elsevier B.V.

1. Introduction

Wildfire dramatically alters the short-term hydrological response of steep watersheds to high intensity rainstorms and increases the likelihood of flash flooding and debris flows (Cannon, 2001; Shakesby and Doerr, 2006; Cannon and DeGraff, 2009). The chaparral-dominated mountains of southern California are particularly prone to post-fire debris flows. Communities, infrastructure, and important habitats and water resources are frequently located within debris flow pathways. The proximity to debris flow pathways can lead to potential catastrophic consequences. These risks create a need to better understand the mechanisms by which post-fire debris flows initiate in order to improve our ability to predict likelihood and magnitude of the debris flow and mitigate their potential hazards. In particular, further insight is needed into how runoff from high-intensity rainfall transitions to debris flow in steep headwater basins.

In unburned settings, landslides and soil slips often initiate debris flows. In this case, a discrete slope failure mobilizes into a debris flow and travels downslope and into the drainage network (Costa, 1984; Johnson and Rodine, 1984). Infiltration during long duration rainstorms increases pore-water pressure within the soil until the material's shear strength is exceeded, and a Coulomb slope failure occurs (Innes, 1983; Costa, 1984; Reneau and Dietrich, 1987; Iverson, 2000). This type of initiation process is easily identified in the field, as the slope failure produces a discrete landslide scar often located in areas of convergent surface or subsurface flow (e.g., Reneau and Dietrich, 1987; Montgomery et al., 2009).

In recently burned areas, debris flows do not necessarily exhibit a discrete initiation point (Parrett, 1987; Meyer and Wells, 1997; Cannon, 2001). Instead, post-fire debris flows are usually generated from entrainment of material by surface water runoff distributed throughout the watershed. Meyer and Wells (1997) described this process as one of progressive bulking based on their observations of erosion features associated with a post-fire debris flow in Yellowstone National Park. They observed that large areas of shallow (~1 cm) erosion on hillslopes gradually transitioned to deeper rills (1–12 cm in depth). Farther downslope, rills graded into deep, narrow gullies incised into areas

* Corresponding author. Tel.: +1 303 273 8568; fax: +1 303 273 8600.
E-mail address: dstaley@usgs.gov (D.M. Staley).

http://dx.doi.org/10.1016/j.geomorph.2014.02.015
0169-555X/Published by Elsevier B.V.

of convergent flow, which subsequently transitioned to stream channels that were eroded to bedrock. They concluded that increasing sediment concentration in surface runoff ultimately contributed to the transition from clear water flow into debris flow. This process has subsequently been observed in other burned areas throughout the world (Cannon and Reneau, 2001; Cannon et al., 2001a,b, 2003; Nyman et al., 2011; Smith et al., 2012).

Erosion of steeplands after wildfire is considered to be a combination of gravitational processes (raveling and rockfall), raindrop-impact-induced erosion (RIIE), surface wash, expansion of the drainage network through headward expansion of the rill and gully network, fluvial erosion, and erosion by debris flow (Cannon, 2001; Gabet, 2003a,b; Kinnell, 2005; Shakesby and Doerr, 2006; Kean et al., 2011; Lamb et al., 2011; Nyman et al., 2011; Smith et al., 2012). Despite the general consensus that erosional processes during high intensity rainfall are responsible for post-fire debris-flow initiation, disagreement exists regarding what processes are most responsible for contributing sediment to post-fire debris flow. Varying emphasis has been placed on the relative importance of raveling, hillslope erosion and erosion of material stored in channels.

Between the wildfire and the first rainstorm, processes such as raveling and aeolian transport are responsible for the transport of materials downslope and to stream channels. Post-fire raveling rates are significantly higher, as physical and chemical changes in soils tend to decrease cohesion between particles, and the combustion of vegetation releases wedges of sediment trapped behind stems and roots during wildfire (Florsheim et al., 1991; Gabet, 2003b; Shakesby and Doerr, 2006; Lamb et al., 2011). Lamb et al. (2011) concluded that post-fire raveling represents one of the primary mechanisms by which post-fire sediment yield is increased following wildfire in steep terrain. The rapid influx of material to a stream channel provides a significant source of material during subsequent runoff events, and is a primary reason for elevated debris-flow hazard in the first few years following wildfire.

Other studies have recognized the importance of both runoff-related hillslope processes and channel erosion in contributing to the initiation and magnitude of post-fire debris flows (Santi et al., 2008; Smith et al., 2012). Smith et al. (2012) analyzed the distribution of fallout radionuclides in post-fire debris-flow deposits. Their results suggested that runoff-induced erosion of fine sediment from hillslopes was the primary contributor of material for the initial surge of a post-fire debris flow. Subsequent surges were found to contain material primarily eroded from stream channels. Hillslopes were found to contribute 22–74% of the total amount of sampled fine material and represented a significant source of material in post-fire debris-flows. These findings differ from those of Santi et al. (2008), who concluded that stream channels constituted the primary source of material during post-fire debris flows. In their study, volumetric estimates of erosion were based upon sediment bulking rates. Sediment bulking rates were calculated from pre-event estimates and post-event measurements of the cross-sections of channels, gullies and rills in 46 debris-flow producing basins. The authors reported hillslopes and gullies contributed a small fraction of material to post-fire debris flows and the main channel was the primary material source. Although these studies have demonstrated that a variety of processes including ravel, rilling, and channel erosion contribute to debris-flow generation, the relative contribution of material from each process still remains largely unknown.

A major step toward improving our understanding of how post-fire debris flows initiate would be to better constrain the spatial context of the primary sources of material in post-fire debris flows. Advances in multi-temporal terrestrial laser scanning (TLS) methods allow for new means of quantifying spatial and temporal patterns of sediment transport at unprecedented spatial resolution. These data permit measurements of erosion and deposition typically constrained to point, plot, or cross-sectional scales, to be made over the entire extent of a small watershed. TLS data, when combined with geomorphic change detection methods, have proven to be a useful tool for interpreting sediment transport rates and processes in fluvial or debris-flow systems (Heritage and Hetherington, 2007; Milan et al., 2007; McCoy et al., 2010; Wheaton et al., 2010; Schurch et al., 2011; Staley et al., 2011), on landslides (Jaboyedoff et al., 2009, 2012), on hillslopes (Hancock et al., 2008), and in recently burned watersheds (Schmidt et al., 2011; Wester et al., 2014).

The spatial domains of various geomorphic processes have previously been defined through morphometric analyses of drainage basins (Evans, 1987; Dietrich et al., 1993). In particular, the form of the relation between contributing area (A_s) and local slope (S_l) has frequently been used to spatially differentiate locations where channelized processes (fluvial or debris-flow incision) are dominant from those where diffusive or hillslope processes are dominant (e.g., Beven and Kirkby, 1979; Willgoose et al., 1991; Tarboton et al., 1992; Montgomery and Foufoula-Georgiou, 1993; Montgomery and Dietrich, 1994; Willgoose, 1994; Ijjasz-Vasquez and Bras, 1995; Prosser and Abernethy, 1996; Prosser and Rustomji, 2000; Millares et al., 2012). Segregating a drainage basin into hillslope and channelized components through this type of analysis then provides a spatial context for the types of erosional processes predicted at a given location. When detailed data regarding the magnitude and spatial distribution of the erosional response during a post-fire debris flow are combined with morphometrically defined elements of the landscape, further insight will be gained into the relative importance of different types of erosional processes. These measurements may then be used to ascertain the primary sources of material and dominant erosional processes that contribute to post-fire debris-flow initiation.

In this study, high-resolution measurements of topographic changes from a debris-flow producing rainstorm are combined with the morphometric analysis of a small headwater drainage basin to: (1) quantify the spatial extent and volume of eroded material using multi-temporal TLS data, (2) segregate the watershed into spatial process domains through morphometric analysis, and (3) use the morphometrically defined process domains to make inferences regarding the primary processes that contribute to debris-flow initiation. Specifically, we use ultra-high resolution (2.5 cm) TLS data to measure the topographic changes during the analyzed rainstorm in a small, steep 0.01 km^2 headwater basin in southern California. We then differentiate, morphometrically, between hillslope-divergent, hillslope-convergent, transitional, and channel locations using traditional area–slope analysis combined with the calculation of planimetric curvature in hillslope areas. The results of the morphometric analysis compare favorably with a geomorphic map based upon repeat TLS data, therefore lending credence to the morphometrically defined process domains. We are then able to calculate the volumetric contributions from each process domain and make inferences regarding the erosional processes responsible for post-fire debris-flow initiation. In doing so, this study provides strong constraints for developing process-based models of important post-fire erosional processes, which can, in turn, lead to improved predictions of debris-flow initiation and magnitude.

2. Study area

This study analyzed a small (0.01 km^2) headwater sub-basin of the Arroyo Seco, which burned during the September 2009 Station fire (Fig. 1). This fire was the largest recorded fire in Los Angeles County history where nearly 65,000 ha of the San Gabriel Mountains were burned between 03 September and 16 October 2009. The San Gabriel Mountains are characterized by a cycle of fire followed by a period of flooding and debris flows, i.e., the "fire–flood sequence" after Hamilton et al. (1954), with a mean recurrence interval on the order of 22–37 years (Lamb et al., 2011). Post-fire erosion processes including debris flows are considered to be one of the primary drivers of long-term evolution of the San Gabriel Mountains (Lavé and Burbank, 2004).

Our study site is located on the eastern flank of Mount Lukens above La Crescenta–Montrose, CA, USA (Fig. 1A). Ninety-nine percent of our

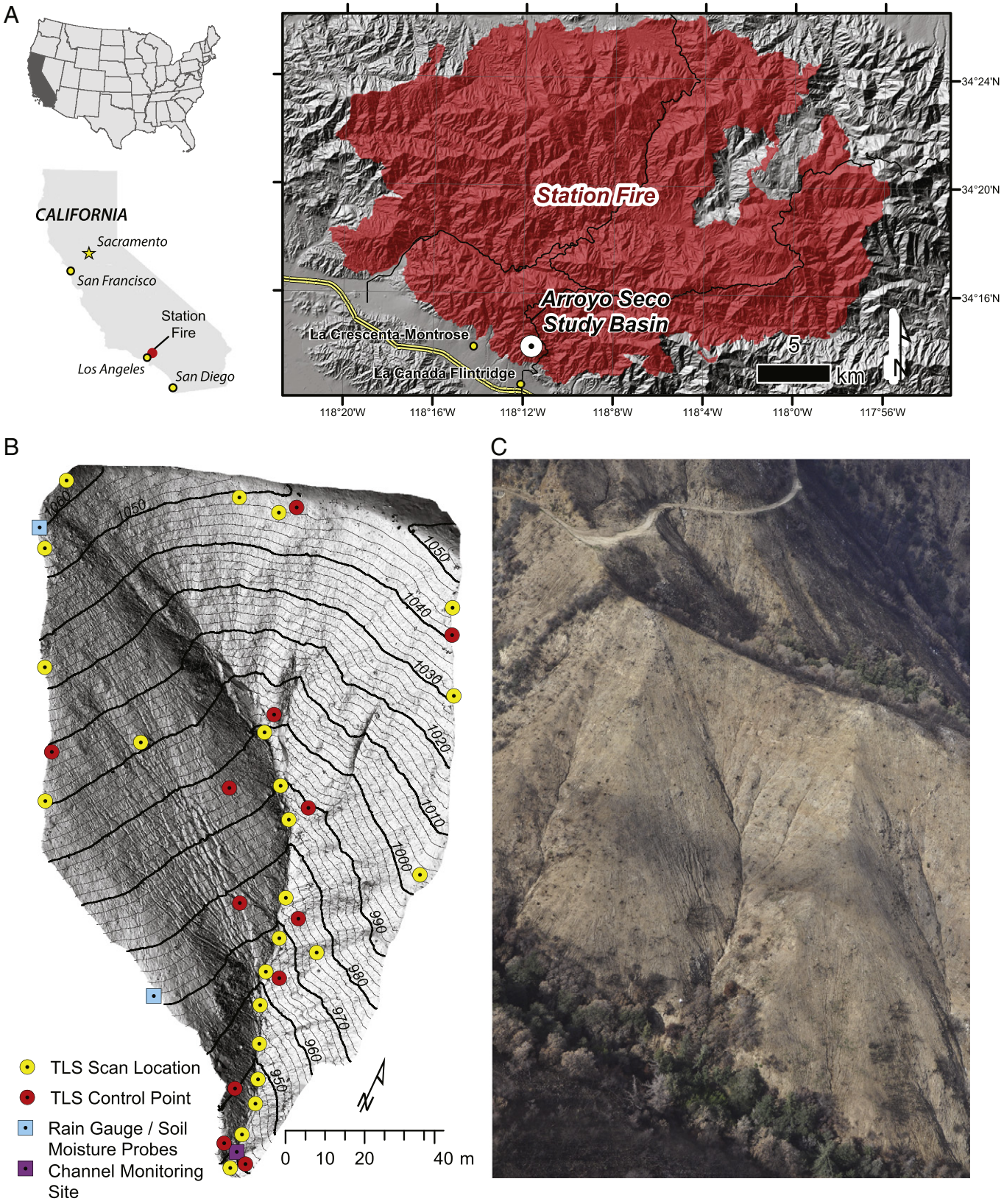

Fig. 1. The Arroyo Seco study basin. (A) Overview of the location of the study area within California and the Station fire. (B) TLS survey information including instrument setup and control point locations. Elevation values are relative to sea level, contour interval = 2 m. (C) Oblique aerial photograph of the study basin, taken on February 2010.

study basin was burned at moderate to high severity (Kean et al., 2011). This region of the San Gabriel Mountains has produced numerous destructive post-fire debris flows, including those during the winters of 1928–29, 1933–34, 1968–69, and 1977–78 (Chawner, 1935; Eaton, 1935; Doehring, 1968; Scott, 1971; McPhee, 1989; Cannon et al., 2011). Debris flows during a series of four storms during the winter of 2009–2010 were recorded within the study basin (Kean et al., 2011; Schmidt et al., 2011). The topographic changes analyzed in this study

were a result of the second debris-flow producing storm of the season. Erosion and deposition during the first debris-flow producing rainstorm are described by Schmidt et al. (2011), and include deep rilling and gullying of soil mantled hillslopes and significant erosion of the main channel. Field observations while working in the study site suggest that a significant volume of material was transported from hillslopes to the gullies and channel by raveling processes between the first and second debris-flow producing rainstorms. The topographic changes documented in this paper incorporate measurements of pre-event ravel transport between the first survey and the debris-flow event. Post-storm raveling between the rainstorm and subsequent survey was considered to be minor based upon our field observations and measurements.

We documented the spatial extent of exposed bedrock and mapped the depth of colluvium at the site during field visits between the end of the fire and the first storm. Bedrock in the study basin is characterized as late Cretaceous granitic rocks (Yerkes and Cambell, 2005), which weather to produce sand and silty-sand textured soils with an average soil dry bulk density of 1940 kg m^{-3}. From our interpretation of post-event aerial and terrestrial photography (Fig. 1C), we estimated that exposed bedrock covered approximately 25% of the basin area. A thin (1–25 cm) mantle of colluvium composes approximately 10% of the basin area. The rest of the basin (~65%) consists of thicker colluvium between 25 and 100 cm deep. Estimates of soil depth were based on season-long observations of erosion in the study basin. Exposed bedrock was highly weathered and easily eroded during rainfall. In certain areas, rills developed on bedrock exposures during the winter season.

The debris-flow producing storm for which we documented topographic changes began on 10 December 2009 and lasted 61 h ending on 12 December 2009 (Fig. 2). Tipping bucket rain gauges installed within the study basin (Fig. 1B) recorded 240 mm of cumulative rainfall and a peak 30-minute rainfall intensity of 23 mm h^{-1} (Fig. 2). This storm was above regional rainfall intensity–duration thresholds for post-fire debris-flow initiation (Cannon et al., 2008, 2011; Staley et al., 2013).

Channel monitoring equipment, including a laser stage gauge and a pressure transducer (see Kean et al., 2011, for additional details) installed in the channel bed (Fig. 1B) recorded seven major periods of debris flow during the storm punctuated by periods of little or no flow in the channel (Fig. 2). Given the lack of flow between debris-flow surges, we consider transport by debris flow to be the dominant mechanism by which material was removed from the study basin during the analyzed rainstorm. Debris flows were detected beginning at 14:48 on 12 December 2009. Each period of debris flow consisted of multiple surges, and the timing of each set of surges was well correlated with peaks in short duration (<15 min) rainfall intensity (Kean and Staley, 2011; Kean et al., 2011, 2012; Staley et al., 2013). The local peaks in 15-minute rainfall intensity associated with each period of debris flow were 22.4, 17.6, 16.0, 16.0, 19.2 and 24 mm h^{-1}. Hillslopes remained unsaturated throughout the rainstorm, where volumetric soil moisture content measurement (θ) from Decagon EC-5 probes installed in the study basin (Fig. 1B) at a depth of 5 cm recorded a maximum value of 0.22 at 18:30 on 12 December 2009 (Fig. 2).

3. Review of morphometric analysis

Over long time scales, the form of a drainage basin reflects the legacy of geologic and geomorphic processes, but over shorter time scales, surface form influences the types of processes at a given location (Schumm and Lichty, 1965; Lane et al., 1998). Investigations into geomorphic process mechanics over short time scales consider topography to be an independent variable which partially controls the rate, magnitude, location and timing of the process. Over longer time scales, the topographic evolution of a hillslope, drainage basin or landscape is often considered to be a dependent variable related to uplift, sediment discharge, lithology, climate, glaciation–deglaciation and erosional process. Often, mathematical models of different types of geomorphic processes are developed to test for characteristic forms or topographic signatures within the landscape that match real-world topography (Kirkby, 1971; Tucker et al., 2001; Stock and Dietrich, 2003; May, 2007). Numerous studies have illustrated the significance of the relational form between contributing area and local slope in determining the dominant geomorphic processes or transport mechanisms that sculpt a drainage basin or landform (e.g.,

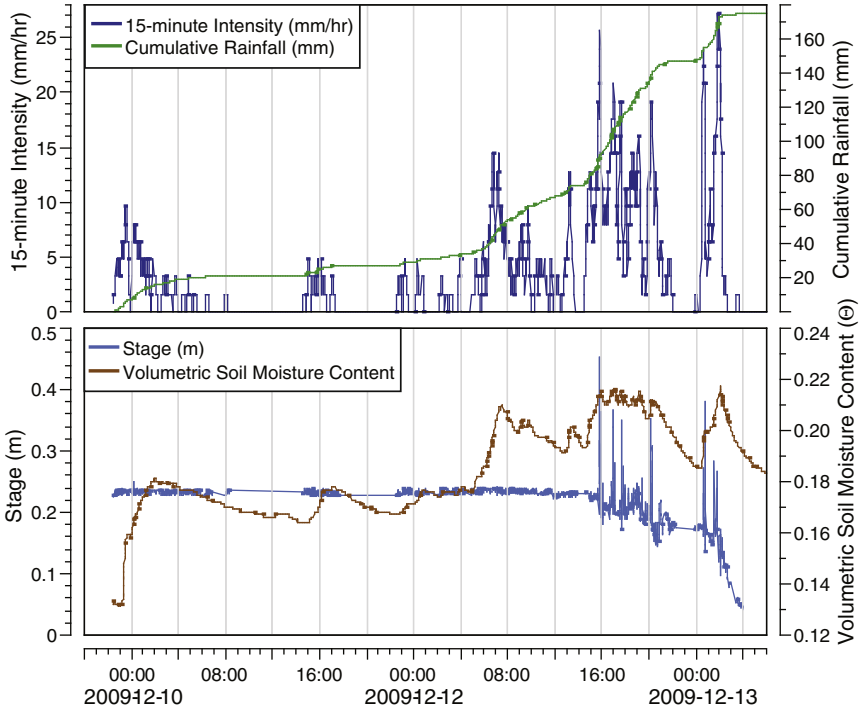

Fig. 2. Hydrological (flow stage and hillslope soil moisture content at 5 cm depth) and meteorological (cumulative rainfall and 15-minute rainfall intensity) data from the 10–12 December 2010 rainstorm which initiated several debris flow surges beginning at 14:29 on 12 December 2010.

Montgomery and Dietrich, 1989; Willgoose et al., 1991; Dietrich et al., 1992, 1993; Montgomery and Foufoula-Georgiou, 1993; Montgomery, 2001; Stock and Dietrich, 2003; Moody and Kinner, 2006). For example, Montgomery and Foufoula-Georgiou (1993) identified four partitions within the area–slope curve, which represented diffusion dominated hillslopes, unchannelized valleys, debris-flow dominated channels, and fluvial channels. In addition, surface curvature has also been identified as a primary morphometric characteristic that both influences and reflects the type of processes that occur at a given location (Blaszczynski, 1997; Stefano et al., 2000; Staley et al., 2006; Minár and Evans, 2008; Bagheri Bodaghabadi et al., 2011; Hurst et al., 2012).

In this study, we utilize area–slope analysis to segregate the drainage basin into domains dominated by channelized processes, such as fluvial transport and debris-flow transport, and domains dominated by hillslope processes. We further segregate the hillslope domain, identified in the area–slope analysis, into divergent and convergent components based upon surface curvature.

3.1. Area–slope analysis

The shape of the area–slope curve for our small, steep study site is formed by two groups of processes for which relative importance is dependent upon the occurrence of wildfire. In between fires, when the site is vegetated, diffusion processes such as soil creep are dominant on the hillslope, while the incisional processes of saturation overland flow, fluvial incision and occasional shallow landsliding sculpt channels. Following the removal of vegetation by periodic fires, other hillslope diffusion processes, including dry ravel and RIIE, greatly increase in importance on the hillslopes (Lavé and Burbank, 2004). In addition, the disturbance of fire permits incision of the hillslopes by overland flow, in the form of rilling and sheetflow erosion. Farther downslope, the channels are carved by increased post-fire runoff that often transforms into debris flows. These post-fire processes are most active in the first year after the fire and diminish with time as vegetation becomes reestablished (typically about 2 years for the study area).

Wildfire disturbs the landscape such that the dominant erosional processes vary in both time and space. For example, increases in runoff may cause rills or gullies that may extend higher onto hillslopes (Moody and Kinner, 2006). Here, we do not attempt to differentiate between specific process domains such as landsliding and overland flow using theoretical thresholds for channelized erosion (e.g. Montgomery and Dietrich, 1994). Instead, the bin-averaged area–slope data were used to identify three more general process domains shown in Fig. 3: hillslopes (Region I in Fig. 3), channels (Region III), and the transitional zone between channels and hillslopes where both process types likely occur (Region II). We define the hillslope domain using the commonly observed reversal point in the trend of the area–slope curve relation. The hillslope domain of the area–slope curve is described by a power law of the form

$$S_l = cA_s^{\ b} \tag{1}$$

where S_l is local slope, A_s is contributing area, c is an empirical constant that incorporates information related to lithology and climate, and b is an empirically defined exponent, which is usually positive.

To the right of the reversal point, channel processes tend to dominate and the trend in the area–slope curve has an inverse relation. This part of the curve can have one or more inflection points that coincide with changes in the dominant erosional process (Montgomery and Foufoula-Georgiou, 1993; Stock and Dietrich, 2003, 2006). Channels dominated by fluvial erosion often follow a power law of the form of Eq. (1) but with a negative exponent b. Channels dominated by debris-flow erosion often have a less steep area–slope relation than fluvial channels, and this relation has been argued by Stock and Dietrich (2003, 2006) to be best fit using a curvilinear function of the form

$$S_{lc} = \frac{S_0}{(1 + c_1 A_s^{\ c_2})} \tag{2}$$

where S_{lc} is the critical local slope, S_0 is the gradient at the reversal point between hillslope and incisional processes, and c_1 and c_2 were empirically derived. Since our basin experiences both floods and debris flows, we evaluated both the fit of a power law and Eq. (2) to the area–slope curve. Given the small size of our basin, we do not expect to see any process-defining inflection points in the area–slope curve at this scale; however, such inflection points may exist if the area–slope analysis was extended beyond the study reach. To further differentiate channelized portions of the reach, we identify fully channelized portions of the study area as those that plot at or above Eq. (2) and transitional areas as those portions of the study area that plot below Eq. (2) (Fig. 3).

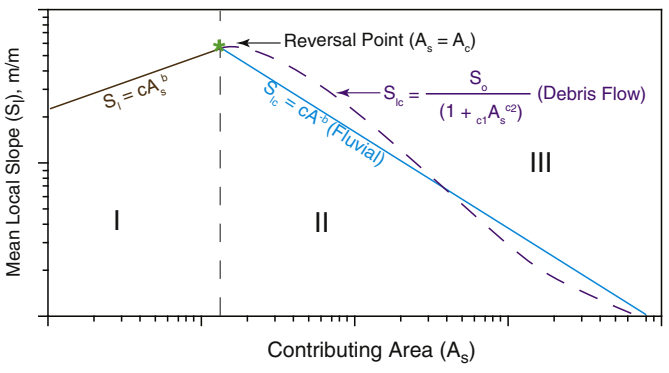

Fig. 3. Idealized area–slope curve for a hypothetical drainage basin. The area–slope curve defines three regions: Region I represents locations dominated by hillslope processes, Region II represents a transitional domain between hillslopes and channels, and Region III represents locations where channel forming processes are dominant. The brown line represents the power law model for hillslope areas, the light blue line represents the power law model for the threshold location of channelized erosion, and the purple line represents Stock and Dietrich's (2003) curvilinear function for the topographic signature of debris-flow incision.

3.2. Surface curvature

At the scale of an individual erosion event, planimetric (cross-slope) curvature strongly influences the flow characteristics at a given location (Evans, 1972; Zevenbergen and Thorne, 1987; Blaszczynski, 1997; Stefano et al., 2000; Moody and Kinner, 2006; Hurst et al., 2012). Flow is divergent in areas characterized by convex planimetric curvature, such as on ridges or nose slopes. Divergent flow produces a downslope decrease in flow depth and unit discharge, in turn producing decreased boundary shear stress. Therefore, areas of divergent flow are not as susceptible to erosion by these processes. Instead, erosion by raveling, RIIE and surface wash would be considered to be more likely dominant in areas of convex planimetric curvature. Conversely, areas characterized by concave planimetric curvature reflect locations of convergent flow. Flow depth and discharge increase in the downslope direction in these areas, thereby increasing the boundary shear stress and producing an increased importance of erosion by overland and concentrated flow processes. In addition, increases in flow depth reduce the influence of raindrop-impact induced erosional processes (Kinnell, 2005). In this paper, we further subdivide the hillslope region of the area–slope curve, where b of Eq. (1) ≥ 0, into concave and convex locations in order to assess the relative dominance of the different types of erosion processes that are partially controlled by planimetric curvature.

4. Methods

4.1. TLS survey

This study relied upon a pre- and post-storm TLS surveys that documented the topographic changes in response to a debris-flow producing rainstorm that spanned 10–12 December 2009. TLS data of the study basin were collected using a Leica ScanStation 2 laser scanner. The first survey was conducted from 22 to 24 November 2009 and the second from 27 to 29 December 2009.

Accurate depiction of fine-scale changes in surface elevation between surveys requires multiple scan locations and a robust control network. Scans recorded at multiple instrument setup locations (see Fig. 1B) were necessary to reduce the number of data voids associated with surface shadowing and achieve a consistent, high density of points. Each survey consisted of scans from 23 different locations, producing point clouds with average point spacing of 1.1 point cm^{-2} after vegetation points were filtered from the dataset (discussed in Section 4.2). Within the study basin, 11 control points were established, each consisting of a 50 cm length of rebar driven into the ground and cemented in place. Leica Geosystems HDS targets were placed upon each point and were scanned at a high resolution to provide precise *x*, *y*, and *z* coordinates for each control point. The proprietary targets also allowed for the automated registration of multiple scans into a single point cloud. The control network allowed for a highly accurate and precise assessment of TLS error, and allowed for the use of a common Cartesian coordinate system between the two surveys.

4.2. DEM creation and differencing

Post-processing of TLS data included vegetation filtering, surface interpolation, uncertainty assessment, and surface differencing. As the Leica ScanStation 2 only captures single returns, it was necessary to identify and remove the remnants of vegetation from the data using a morphological filter. We used the LASGROUND function of LASTools (Isenburg, 2012) to extract bare-Earth points from the raw data using the following parameters: Step = 0.05 m, Spike = 0.1 m, and Offset = 0.1 m, where step represents the size of the analysis window, spike represents the minimum elevation change within the analysis window used to detect potential vegetation points, and the offset parameter classifies the maximum value above the ground estimate at which potential vegetation points will be classified as ground (Isenburg, 2012). The parameter values were selected using an iterative process where model outputs were examined at selected sites within the study basin. We then created a temporary TIN of the bare-Earth points. Given the high density of the filtered point cloud, the TIN data model was considered to be the optimal means of surface creation as the exact value of the data points are used as TIN vertices, and are not interpolated (as with other methods such as Kriging or Inverse Distance Weighting interpolation methods). The TIN was then resampled to a 2.5 cm resolution DEM using bilinear interpolation. Raster data were imported into ArcGIS for further analysis.

Topographic changes between scans were calculated by creating a DEM of Difference (DoD), where the DEM of the pre-storm surface was subtracted from that of the post-storm DEM surface (Fig. 4). Positive values indicated areas of deposition, whereas negative values indicated areas of erosion. Volumetric change, ΔV, was calculated as:

$$\Delta V = \frac{A_v \times \sum_{(i,j)=1}^{n} \Delta Z_{(i,j)}}{n} \tag{3}$$

where A_v = area over which volume is being calculated (m^2) and $\Delta Z_{(i,j)}$ = change in elevation at pixel (i,j) (in m) and n = the total number of pixels in A_v.

4.3. Uncertainty assessment

Uncertainty in the measurement of topographic change is a function of the accuracy of the point cloud, point density, surface complexity and the interpolation method (Heritage et al., 2009; Wheaton et al., 2010; Milan et al., 2011). These uncertainties are compounded at each step in the analysis, and must be taken into account when assessing the magnitude and direction of surface change and in subsequent volumetric calculations. We rely upon a spatially uniform uncertainty assessment that statistically defines the minimum level of detection (Brasington et al., 2003; Lane et al., 2003; Bennett et al., 2012). We do this by (1) assessing the accuracy of the point cloud data and derived surface for each survey, (2) propagating the uncertainty from both surveys into the DoD, and (3) determining the significance of the propagated uncertainty on volumetric measurements obtained by the DoD (Brasington et al., 2003; Lane et al., 2003; Wheaton et al., 2010; Bennett et al., 2012). Uncertainties in the raw point cloud data can arise in the direction of *x*, *y*, and *z*. Vertical (z) uncertainties significantly influence DEM quality and DoD measurements at lower gradients, whereas horizontal (x and y) uncertainties are more significant at higher gradients. To account for all of these potential sources of uncertainty, we calculate systematic error (*SE*) and the standard deviation (σ) of error as measured at control point locations (Table 1). *SE* measures potential bias or directionality in survey measurements (e.g., measurements that are consistently high or consistently low), whereas σ provides a more robust measure of overall uncertainty (Taylor, 1982).

Accurate assessment of geomorphic change relies upon a robust strategy to determine the minimum level of detection (Lane et al., 2003). We determine the minimum level of detection by first quantifying our errors in *x*, *y*, and *z* based on the standard deviation of errors at the control points:

$$\sigma = \sqrt{\frac{1}{M}\sum_{p=1}^{M}\left(\delta_p - \mu\right)^2} \tag{4}$$

where M = the number of control points, δ_p = the error at control point p (in *x*, *y*, or *z* directions), and μ = the mean uncertainty at all control points (calculated individually for *x*, *y*, and *z* directions). We then propagate the errors in *x*, *y*, and *z* using the equation:

$$\delta_z = \sqrt{(\sigma_{x1})^2 + (\sigma_{x2})^2 + (\sigma_{y1})^2 + (\sigma_{y2})^2 + (\sigma_{z1})^2 + (\sigma_{z2})^2} \tag{5}$$

where subscripts *x*, *y* and *z* represent directional uncertainty, and subscripts 1 and 2 represent surveys 1 and 2, respectively. To statistically define the threshold value for the minimum level of change, we calculate the *t*-statistic at each pixel:

$$t = \frac{\left|\Delta Z_{i,j}\right|}{\delta_z}. \tag{6}$$

A cumulative distribution function of t was then derived for the *t*-statistic surface, and only those pixels where $t > t_c$ (critical t = minimum level of detection) were considered to have a magnitude of topographic change that exceeded the minimum level of detection based upon our uncertainty analysis. We chose t_c to be 1.96 based on an alpha = 0.95 significance level. Only those pixels that were identified to exceed the minimum level of detectable topographic change (±0.011 m) were included in the volumetric analysis.

We continued to follow the methods of Lane et al. (2003) to determine the uncertainties found in the volumetric calculations, where volumetric error (δ_v) is defined using δ_z such that:

$$\delta_v = \delta_z \times A_v. \tag{7}$$

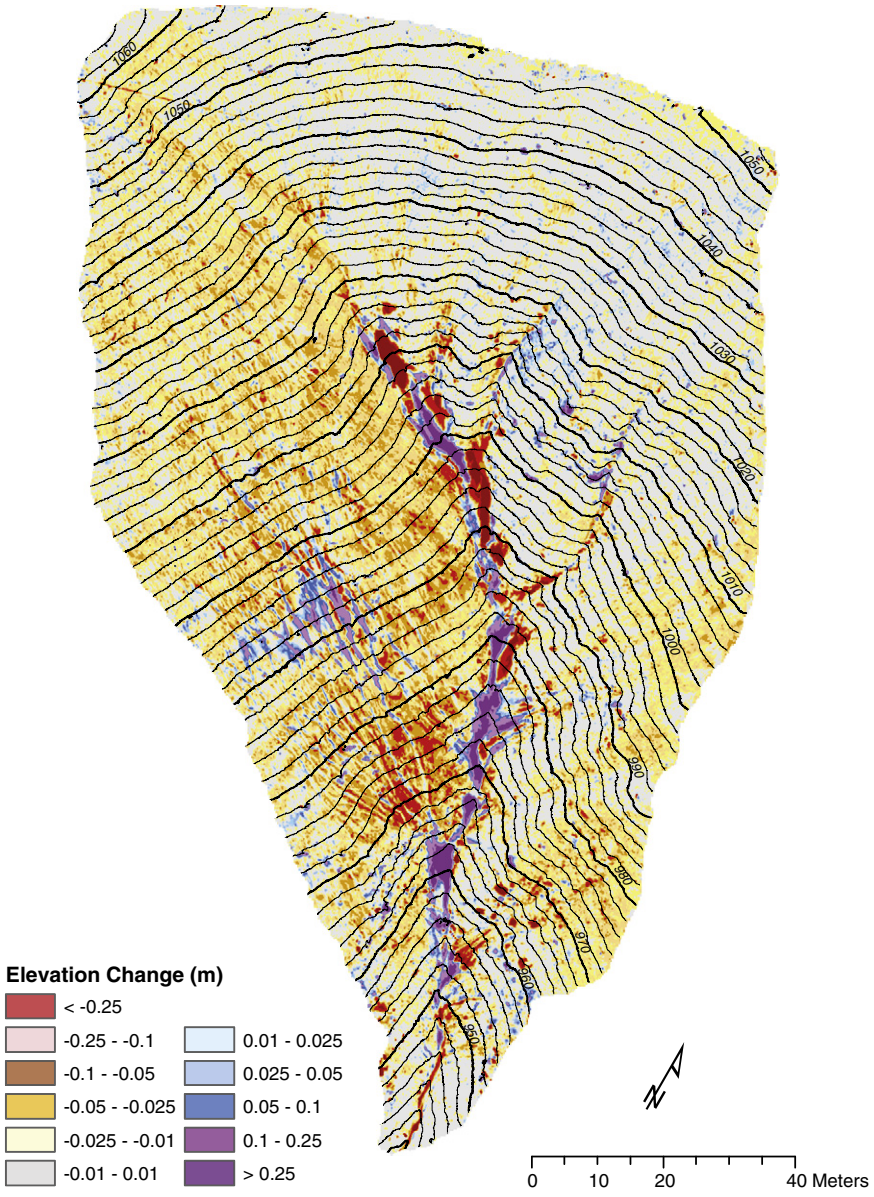

Fig. 4. Topographic changes measured from multi-temporal TLS surveys in the Arroyo Seco study basin. Negative values (red and yellow shades) indicate erosion. Positive values (blue and purple shades) indicate deposition. Elevation values are relative to sea level, contour interval = 2 m.

Values are reported after calculated volumes as ± values representing the upper and lower limits of estimated volumetric error. We calculated erosion, deposition, net erosion volumes, and associated uncertainties separately.

4.4. Elevation derivatives

This study relies upon the morphometric attributes of A_s, S_l, and planimetric curvature (k). For the calculation of each metric, we

Table 1
TLS uncertainty values for control points. Survey 1 was 22–24 November 2009 and Survey 2 was 27–29 December 2009. *SE* = systematic error, σ = error standard deviation, $>t_c$ = minimum level of detection ($t > 1.96$, $\Delta Z \geq 10.1$ mm). Note that all uncertainty values are in millimeters.

Coordinate direction	Uncertainty metric	Survey 1 uncertainty (mm)	Survey 2 uncertainty (mm)	Propagated uncertainty (mm)
X	*SE*	0.01	0.05	0.05
	σ	±1.23	±1.47	±1.92
Y	*SE*	0.02	−0.03	0.03
	σ	±1.96	±1.56	±2.51
Z	*SE*	0.00	0.04	0.04
	σ	±1.98	±1.86	±2.71
All (*X*, *Y* and *Z*)	*SE*	–	–	0.07
	σ	–	–	±4.16
	$>t_c$	–	–	±10.1

resampled the 2.5 cm DEM created during the previous analysis to a resolution of 10 cm. We selected a resolution coarser than the original resolution in order to minimize the effects of fine-scale (1 cm) variations in local topography (e.g. rocks, roots and stumps), while preserving the medium-scale (10 cm) topographic features that influence the hydrology of the basin, such as bedrock outcrops, swales, and channel banks.

The d-infinity flow algorithm (Tarboton, 1997) was used to calculate A_s. S_l was defined as the rate of maximum change of elevation within a 50 × 50 cm analysis window. k was calculated using a 30 × 30 cm analysis window following the methods of Blaszczynski (1997) and Staley et al. (2006). S_l and k were both calculated from a 10 cm DEM that had been smoothed using a nonlinear diffusion filter (Passalacqua et al., 2010a). A nonlinear diffusion filter was selected for DEM conditioning as this smoothing method has been demonstrated to achieve noise reduction while avoiding unnecessary smoothing across natural boundaries and preserving important natural edges, such as stream banks or rills (Passalacqua et al., 2010a,b).

4.5. Area–slope curve

S_l was calculated as bin averages for each 0.10 log interval of contributing area (e.g., 1, 2, 3…10, 20, 30…100, 200, 300 m^2). We then fit trends to the hillslope and channel portions of the area-curve. For the hillslope trend, we first fit a simple power-law equation (Eq. (1)) to all of the area–slope data. Larger drainage areas were successively removed until the gradient of the line turned positive. The largest remaining area was defined as the critical contributing area, A_c, which we considered to be the transition point between hillslope and channel process domains. For the remaining data (where $A_s > A_c$), we fit both a power law and the curvilinear equation of Stock and Dietrich (2003) (Eq. (2)).

4.6. Geomorphic mapping

We spatially constrained the extent of geomorphic processes by mapping the location of easily recognizable geomorphic features (both erosional and depositional) such as ravel deposits, rills, fluvial deposits, and debris-flow deposits (Fig. 5). The map was used for documenting

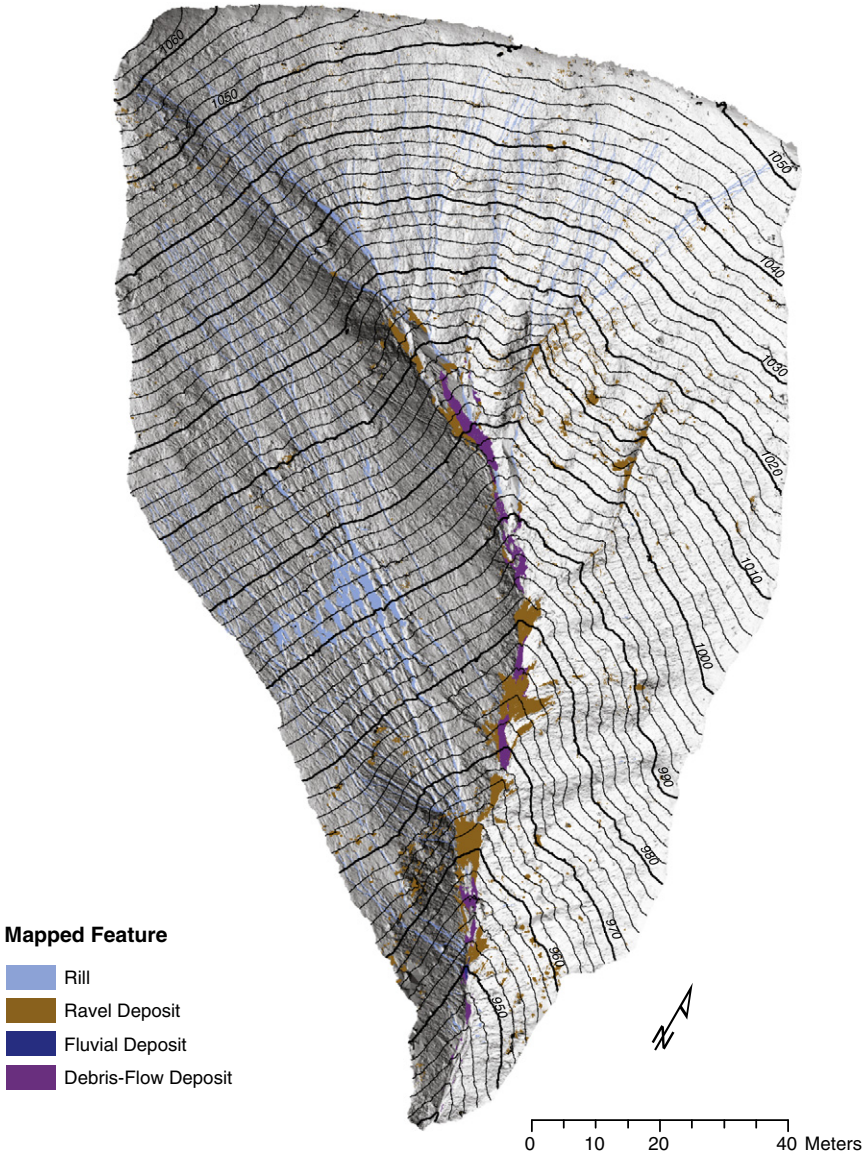

Fig. 5. Geomorphic map of the study basin identifying rills, ravel deposits, fluvial deposits and debris-flow deposits. Rill heads were mapped from hillshaded DEM data; deposits were mapped using field methods, change detection data and terrestrial photography.

the occurrence of each process type and references their location in relation to A_s, S_l, and k. With the exception of rilling, it was impossible to differentiate the process type that caused erosion at a given location. For example, there is no way to differentiate from post-event imagery or reconnaissance if erosion in the stream channel was caused by debris-flow processes or fluvial incision during the recessional flow. Similarly, on hillslopes, it is impossible to determine the relative contributions of ravel, RIIE, and surface wash to erosion.

Rill erosion was mapped because this process produces easily recognizable linear features on hillslopes. For a representative sample of 59 rills, we calculated rill length from head to the main channel using the d-infinity flow accumulation algorithm (Tarboton, 1997). Discontinuous rills (i.e., rills that stopped short of the main channel) were not mapped, as the location of these transient features could not be adequately determined from flow modeling.

Depositional features have distinct morphometric and sedimentological characteristics, which allow interpretation of the process types responsible for their formation. Deposits were mapped using a combination of TLS data, imagery and field mapping. Material accumulations with a minimum depth of 5 cm that occupied at least 0.05 m^2 represented the smallest depositional unit within the geomorphic map. Deposits that failed to meet the minimum depth or area criteria were recorded as "unclassified." Deposition exceeding the minimum mapping criteria was divided into four groups: dry ravel deposition, rill deposition, fluvial deposition and debris-flow deposition. Dry ravel transport forms wedge- or cone-shaped deposits of fine material at a gradient slightly less than the angle of repose (friction angle [φ] = 41° in the study basin, after Kean et al., 2011), or as wedges of material accumulated at the base of vegetation remnants or in topographic concavities (Lamb et al., 2011). Fluvial deposits were identified in the main channel and were differentiated from other deposit types based upon degree of stratification and sorting (Cannon, 2001). Debris-flow deposits were distinguished from fluvial deposits as they were matrix-supported with random clast orientations (Cannon, 2001) and often had a characteristic levee or lobate shape (see Fig. 5).

5. Results

5.1. Morphometric analysis

The area–slope curve and surface curvature measurements were used to morphometrically define four process domains (Table 2). Hillslope locations were separated from transitional and channelized incision locations at the slope reversal point corresponding to $A_s = 100$ m^2 and $S_l = 0.85$ (Fig. 6). Where $A_s \leq 100$ m^2, the data were best fit by the power law:

$$S_l = 0.81 A_s^{0.009} \tag{8}$$

with an r^2 value of 0.76 and randomly distributed residuals. The positive exponent indicated that slope increased with gradient until the threshold was reached at $A_s = 100$ m^2. Within this process domain, we hypothesize that hillslope processes represent the primary mechanisms for erosion. To further segregate the hillslope process domain, we separated locations by k to differentiate areas of convergent and divergent flow (Fig. 6) and infer their primary erosional processes (Table 2).

Assuming that the location where erosion by incisional processes is dependent upon local slope, the reversal point at $A_s = 100$ m^2 and $S_0 = 0.85$ represents the minimum critical support area and local slope for channelization by fluvial and debris-flow processes. Where $A_s > 100$ m^2, the bin-averaged slope values were best represented by the equation:

$$S_{lc} = \frac{0.85}{1 + 0.0006 A_s^{0.69}} \tag{9}$$

which had an r^2 value of 0.77 and randomly distributed residuals. Fitting a power law to the same data yielded a slightly lower r^2 value of 0.70 and a non-random distribution of residuals.

The transition from hillslopes to channelized processes occurs in the region of the area–slope curve where $A_s > A_c$ and the data are best fit by Eq. (9) (Willgoose et al., 1991; Montgomery and Foufoula-Georgiou, 1993; Montgomery and Dietrich, 1994). We chose to use Eq. (9) to represent the boundary between transition zones ($S_l < S_{lc}$) and fully channelized portions of the study area ($S_l > S_{lc}$). The transitional process domain contains evidence of both hillslope processes and channelized incisional processes; the extent and precise location of each process type would be dependent upon evolving local conditions, rainfall characteristics and runoff generation. We applied the above criteria to the pre-event DEM to produce a map of the four process domains (Fig. 7).

5.2. Validation of process domains

The validity of the morphometrically defined process domains was assessed by comparing the location of deposits identified in the geomorphic map with our interpretations of the area–slope and curvature analysis. The spatial accuracy of our interpretations were assessed by comparing the percentage of mapped feature area (Table 3) and percentage of mapped and classified deposit volume (Table 4) within each process domain.

For rills, 51.9% of the mapped rill areas were intuitively located in the hillslope-convergent process domain, and another 34.2% of the rills extended into the channelized incision process domain (Table 3). Only 7.8% of the mapped extent of rills was found to be located in the hillslope-divergent process domain, and 6.1% within the transitional process domain.

Dry ravel is considered a slope-dependent process (Gabet, 2003b; Lamb et al., 2011) and was clearly evident within the hillslope-divergent and hillslope-convergent process domains. These two process domains composed 76.9% of the mapped ravel deposit area (Table 3) and 69.9% of the total ravel deposit volume (Table 4). The channelized incisional process domain contained an additional 27.0% of the total volume of ravel deposition. Steep hillslope gradients permitted the raveled material to be transported from hillslope locations to lower gradient channel locations, a common occurrence in recently burned mountainous areas (Florsheim et al., 1991; Gabet, 2003b; Shakesby and Doerr, 2006; Lamb et al., 2011).

Fluvial deposits were identified near the mouth of the basin, where contributing area exceeded 12,000 m^2. Seventy-four percent of the total area of fluvial deposits was located within the channelized process domain, whereas 26% were located in the hillslope-convergent process domain (Table 3). A similar percentage was obtained for the total volume of fluvial deposit material, with 73.0% of the deposit volumes

Table 2
Morphometric definition of process domains in the Arroyo Seco study basin where A_s = contributing area (m^2); A_c = critical contributing area of 100 m^2; k = curvature; S_l = local slope ($m\ m^{-1}$) and S_c = critical local slope.

Morphometrically defined process domain	Morphometric definition	Hypothesized process-types	Total area (m^2)	Percent of basin area
Hillslope-divergent	$A_s < A_c$ and $k \leq 0$	Raindrop-impact induced erosion, overland flow, ravel	6182.2	49.8
Hillslope-convergent	$A_s < A_c$ and $k > 0$	Overland flow, rilling	5695.6	45.9
Transitional	$A_s > A_c$ and $S_l < S_{lc}$	Overland flow, rilling, debris flow	131.1	1.0
Channelized incision	$A_s > A_c$ and $S_l \geq S_{lc}$	Debris flow, fluvial	411.0	3.3

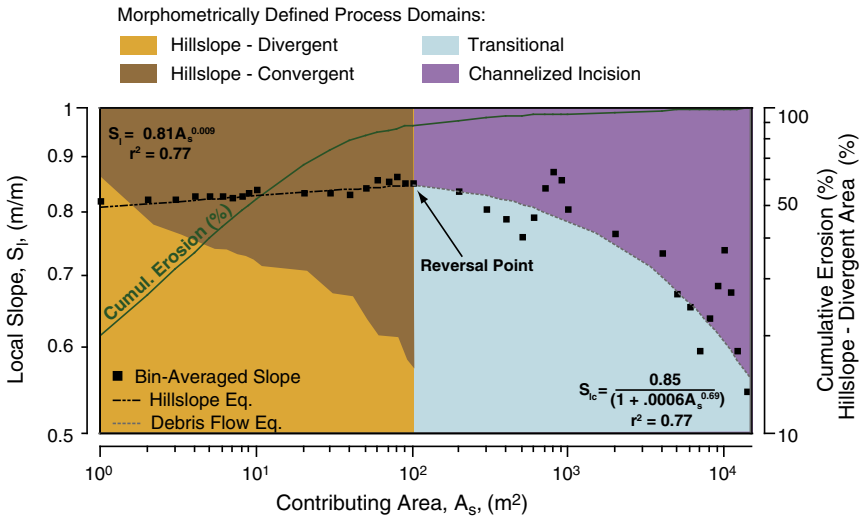

Fig. 6. Plot demonstrating the area–slope relation, erosional thresholds, morphometrically defined process domains and location of mapped features within the study basin. The dark green line represents the cumulative erosion as related to contributing area. The black squares represent bin-averaged local slopes (S_l). The vertical dashed red line represents the contributing area (A_c) defining the boundary between hillslopes and channels. To the left of this point, the dashed black line represents the best-fit equation (power-law equation at the top left) for hillslope locations. To the right of A_c the dashed gray line represents the best-fit equation (curvilinear equation at the bottom right) identifying the erosional threshold for channelized incision, where areas under the curve (light blue) represent the transitional process domain where S_l is less than the critical local slope (S_{lc}). The area above the curve (purple) represents the locations where $S_l > S_{lc}$ and channel incision processes were dominant. The brown and orange colors to the left of A_c relate to the *y*-axis on the right side of the graph, and represent the proportion of area within the hillslope-divergent process domain for each bin of contributing area.

located in channelized incision process domain and 27.0% within the hillslope-convergent process domain (Table 4).

Debris-flow deposits were well constrained to be within the transitional and channelized incision process domains. The upslope-most debris-flow deposits were mapped where $A_s = 101$ m^2, nearly the exact value of the reversal point on the area–slope curve. Most of the mapped debris-flow deposit area (54.3%) was located within the channelized process domain and 37.4% was located in the hillslope-convergent process domain (Table 3). The channelized incision process domain contained -11.7 ± 0.2 m^3 (63.3%) of the total debris flow volume, whereas the hillslope-convergent process domain contained 32.6% (6.0 ± 0.1 m^3) of the total debris flow deposit volume (Table 4).

For a majority of the analyzed deposits, the mapped geomorphic features that would be expected to be located in hillslope areas of convergent flow (rills) or in the transitional or channelized incision process domains (rills, fluvial deposits and debris-flow deposits) were correctly located. From these results, we conclude that the morphometric definition of process domains based upon the area–slope curve produce reasonably accurate estimates of the mapped feature locations. In the following sections, we combine the results of the morphometric analysis with traditional sediment budgeting to define the spatial context of erosion and deposition during the debris-flow producing rainstorm and make inferences regarding the types of processes that may be important for post-fire debris-flow initiation in a steep headwater basin.

5.3. Sediment budget and geomorphic mapping

Topographic changes (ΔZ) (Fig. 4) ranged from -1.34 ± 0.04 m (erosion) to 1.77 ± 0.04 m (deposition). The sediment budget presented here represents the total erosion (E_{tot}), total deposition (D_{tot}), and net erosion ($E_{tot} + D_{tot}$, where positive values represent net erosion) measured within the study basin (Table 5). We calculated a total loss of 313.5 ± 35.9 m^3 of material to erosion, a total deposition of -125.9 ± 15.7 m^3, and a net loss of material to erosion of 187.5 ± 52.3 m^3 within the analyzed basin. These data correspond to a sediment-delivery ratio (net erosion divided by total erosion) of 0.6, a basin-average erosion depth of 1.5 cm, and a sediment yield of 383.8 ± 80.7 t ha^{-1} for the two-month period between surveys based on a field-measured average dry bulk density of 1.1 g cm^{-1}. The sediment yield ranks on the high end of the annual sediment yields for southern California (Moody and Martin, 2009), despite the fact that the monitoring period only contained a single debris-flow producing rainstorm during a winter over which four separate storms produced debris flows in the study basin (Kean et al., 2011). Interestingly, our measured net loss of 187.5 m^3 compares favorably with an indirect estimate of volume for this storm calculated by Kean et al. (2011) (174 m^3). Their estimate was based on the product of estimated debris-flow velocity and the integral of the debris-flow stage hydrograph.

The erosion depth and areal extent provide insight into the dominant processes and sources of material during the debris-flow event. An analysis of the cumulative distribution of material eroded from and deposited within the basin at 1 cm depth intervals indicates that most of the material yielded from the study basin was associated with shallow erosion depths (Fig. 8A). Here, 50% of the material transported from the study basin corresponded to erosion depths of less than 6 cm, and 80% of the material was eroded from depths less than 13 cm. In addition, 50% of the total erosion volume was removed from locations where $A_s \leq 10$ m^2, and 80% of the area was eroded from locations where $A_s \leq 40$ m^2 (Fig. 8B) We interpret these findings to indicate the relative importance of the erosional processes that dominate locations with small contributing areas and that produce a shallow erosional response such as ravel, RIIE, overland flow, and rill erosion. Furthermore, these results indicate that hillslope locations are the primary sources of material for this study site and event.

5.4. Primary sources of sediment

We use the four morphometrically defined process domains to analyze the total erosion, total deposition and net erosion within each process domain to determine the primary sources of sediment and infer the primary transport processes for the analyzed rainstorm.

5.4.1. Hillslope-divergent process domain

This process domain composed 50% (6182.2 m^2) of the total basin area and contributed a majority of the total sediment eroded during the analyzed rainstorm, with a total erosion volume of 179.3 ± 19.0

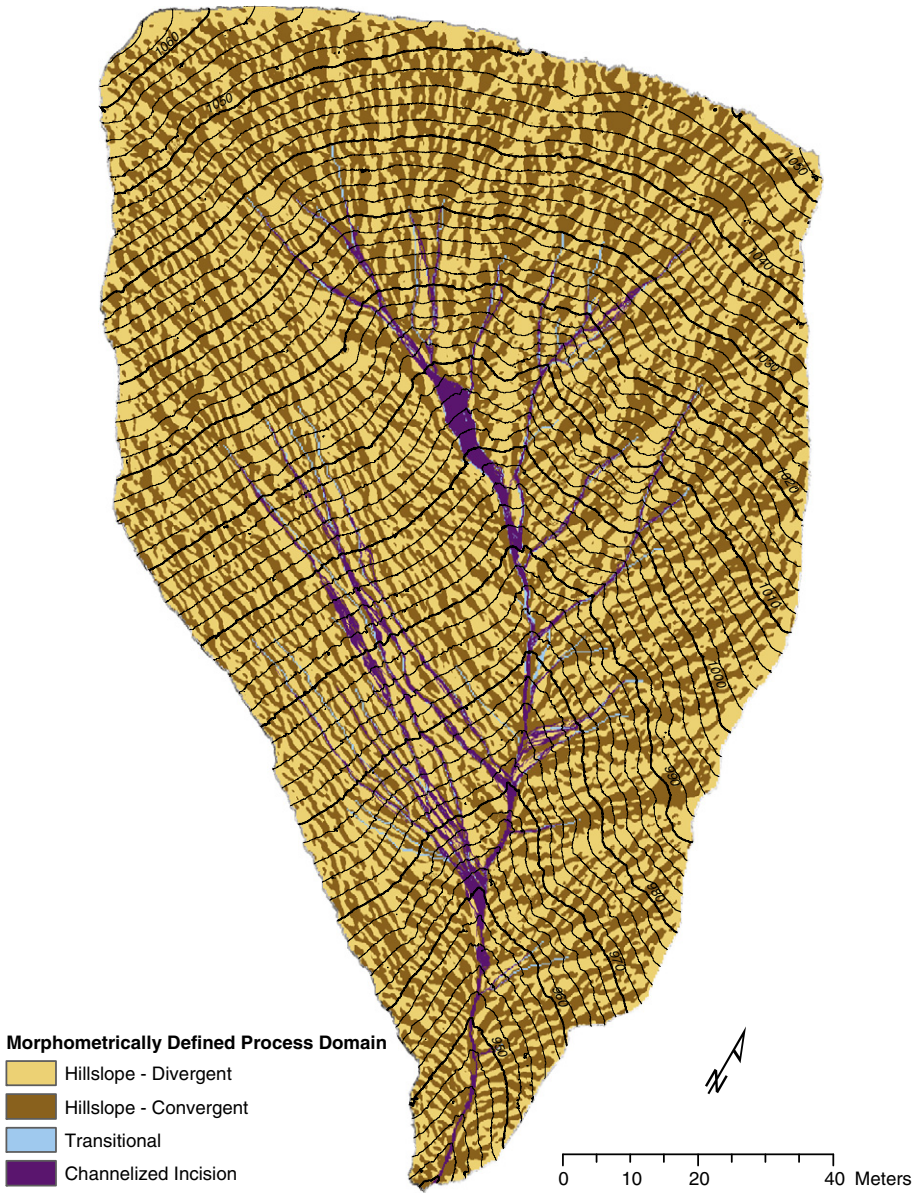

Fig. 7. Morphometrically defined process domains. The hillslope-divergent process domain (light orange) represents locations where contributing area (A_s) < 100 m^2 and curvature (k) < 0. The hillslope-divergent process (brown) domain represents locations where A_s > 100 m^2 k > 0. The transitional process domain (light blue) represents locations where A_s > 100 m^2 and local slope (S_l) is less than the critical value (S_{lc}) determined by Eq. (9). The channelized incision process domain (purple) represents locations where A_s > 100 m^2 and S_l > S_{lc}.

m^3 and with a net erosion of 147.2 ± 26.0 m^3 (Fig. 9 and Table 5). This process domain produced 57% of the total volume of material eroded within the watershed during the study period, with an average erosion depth of 3.9 cm and a sediment delivery ratio of 0.82.

5.4.2. Hillslope-convergent process domain

This process domain occupied 46% (5695.6 m^2) of the study basin and contributed a total erosion volume of 111.8 ± 15.9 m^3 and a net erosion of 53.3 ± 24.0 m^3, contributing 36% of the total volume of material eroded within the basin during the analyzed rainstorm (Fig. 9 and Table 5). Hillslope-convergent locations had an average erosion depth of 2.9 cm and a sediment delivery ratio of 0.47.

5.4.3. Transitional process domain

The transitional process domain occupied 1% (131.1 m^2) of the study basin. We calculated a total erosion volume of 4.5 ± 0.3 m^3 and a net erosion of 1.1 ± 0.5 m^3 (Fig. 9 and Table 5). This process domain had an average erosion depth of 5.8 cm and a sediment delivery ratio of 0.24.

Table 3
Total feature area (in m^2) and percentage of total feature area (in parentheses) of each feature-type within each of the four morphometrically defined process domains.

	Hillslope-divergent	Hillslope-convergent	Transitional	Channelized incision	Total
Ravel deposits	86.8 (29.9%)	136.7 (47.0%)	9.7 (3.3%)	57.4 (19.8%)	290.6 (100.0%)
Rills	9.5 (7.8%)	62.9 (51.9%)	7.4 (6.1%)	41.5 (34.2%)	121.3 (100.0%)
Fluvial deposits	0.0 (0.0%)	0.3 (25.9%)	0.0 (0.0%)	0.8 (74.1%)	1.1 (100.0%)
Debris-flow deposits	3.6 (4.9%)	27.5 (37.4%)	2.5 (3.4%)	40.0 (54.3%)	73.6 (100.0%)

Table 4
Total volume (in m^3) and percentage of total deposit volume of each feature-type within each of the four morphometrically defined process domains.

	Hillslope-divergent	Hillslope-convergent	Transitional	Channelized incision	Total
Ravel deposits	−12.2 ± 0.4	−24.4 ± 0.6	−1.6 ± 0.0	−14.1 ± 0.2	−52.4 ± 1.2
Fluvial deposits	0.0 ± 0.0	−0.1 ± 0.0	0.0 ± 0.0	−0.1 ± 0.0	−0.2 ± 0.0
Debris-flow deposits	−0.4 ± 0.0	−6.0 ± 0.1	−0.3 ± 0.0	−11.7 ± 0.2	−18.5 ± 0.3

5.4.4. Channelized incision process domain

The channelized process domain (411.0 m^2 [3%] of the study basin) acted as a net sediment sink during the analyzed rainstorm, where net erosion was −14.0 ± 1.7 m^3 (negative values of erosion indicate deposition). Deposition from debris flow and (−11.7 ± 0.2 m^3) and raveling (−14.1 ± 0.2 m^3) (Table 4) were primarily responsible for the net deposition calculated in this process domain during the analyzed rainstorm (Fig. 9 and Table 5). Continuous erosion was identified only along the lowermost portion of the channel near the basin outlet. Volumetric change calculations were not made below the confluence with the mainstem where substantial erosion was identified during post-event site visits.

6. Discussion

Hillslope-divergent and hillslope-convergent process domains represent the primary sources of material eroded during the analyzed rainstorm, with measured net erosion volumes of 147.2 ± 26.0 m^3 and 53.3 ± 24.0 m^3, respectively (Fig. 9). Most erosion was associated with shallow depths (<6 cm) and in areas with small contributing areas (<10 m^2) (Fig. 8). Based on this evidence, we conclude processes operating in the hillslope domain, such as ravel, RIIE, surface wash, and, rilling were the primary mechanisms by which sediment was eroded during the monitoring period. As these hillslope processes remove mostly fine material, our findings support the conclusions of Smith et al. (2012). In their study, they used fallout radionuclide tracers to determine the percentage of material that originated on hillslopes in the deposits of post-fire debris flows in Australia. They concluded that hillslopes contributed 32–74% and 22–69% of the analyzed deposition in their study basins. Our findings support their upper range of estimates of fine material contribution from hillslopes.

The transitional process domain constitutes a very small percentage of the total basin area and was found to have the least amount of net erosion of the four morphometrically defined process domains. However, this process domain may be a critical location for the transition from overland flow to debris flow, as these locations may temporarily store sediment during a rainstorm (Kean et al., 2013). A recent study of debris-flow surges observed at the study site (Kean et al., 2013) proposed a model for debris-flow initiation based on the idea that transitions to lower gradient slopes (like those in the transition zone) act as "sediment capacitors," which temporarily store incoming sediment from upstream and periodically release the accumulated material as a debris-flow surge. Their mathematical implementation, the "sediment capacitor" model, qualitatively matched the observed trends in debris-flow surge magnitude and frequency at the site. Our observations are consistent with this model of initiation, in that the upstream-most debris-flow deposit in the catchment was located in the lower gradient transitional region and followed down channel by a series of other lobate deposits indicative of surges. Thin debris flows originating from small Coulomb failures on the hillslopes (e.g., Gabet, 2003a) may also have contributed to hillslope erosion and debris-flow initiation. Schmidt et al. (2011) identified these features in our study basin at contributing areas of 20–30 m^2 during the previous debris-flow event on 12 November 2009. Although further work is necessary to understand the physical mechanisms by which surface runoff transitions to debris flow, the results of this study provide a spatial context within which measurements of flow properties, sediment dynamics and topographic evolution may be made and modeling efforts may be focused.

The channelized process domain acted as a net sediment sink for the analyzed rainstorm. We identified that the onset of continuous erosion of channel material only began near the basin outlet and junction with the trunk stream. If this trend continued downstream, it is possible that with increasing contributing area the relative importance of erosion in channels from debris flows will exceed the contribution of material from hillslopes, and the channel will become the primary source of material. However, the analyzed basin was too small to permit further extrapolation of channel erosion rates, and no measurements of erosion were made along the trunk stream. In light of evidence of continuous channel erosion at contributing areas greater than 12,000 m^2, further work is needed to determine if, where, and when channels become the primary source of material when measured in larger drainage basins, a conclusion reached by Santi et al. (2008). It also should be

Table 5
Summary of domain area, total erosion, total deposition, net erosion and average change in elevation (ΔZ) for the entire drainage basin, and separately for the process domain identified by analysis of the area–slope curve and hillslope curvature. Detectable area (third column from the right) refers to the total area of the topographic changes that exceeded the minimum level of detection where $t > 1.96$ and $\Delta Z > 0.011$ m.

	Location	Detectable area (m^2)	Volumetric change (m^3)	Average ΔZ (cm)*
Total erosion (E_{tot})	Hillslope-divergent	4558.9	179.3 ± 19.0	3.9
	Hillslope-convergent	3815.1	111.8 ± 15.9	2.9
	Transitional	77.2	4.5 ± 0.3	5.8
	Channelized incision	189.2	17.8 ± 0.8	9.4
	Basin total	8640.4	313.5 ± 35.9	3.6
Total deposition (D_{tot})*	Hillslope-divergent	1623.3	−32.2 ± 6.8	−2.0
	Hillslope-convergent	1880.5	−58.5 ± 7.8	−3.1
	Transitional	53.9	−3.3 ± 0.2	−6.2
	Channelized incision	221.8	−31.9 ± 0.9	−14.4
	Basin total	3779.5	−125.9 ± 15.7	−3.3
Net erosion ($E_{tot} + D_{tot}$)*	Hillslope-divergent	6182.2	147.2 ± 26.0	2.4
	Hillslope-convergent	5695.6	53.3 ± 24.0	0.9
	Transitional	131.1	1.1 ± 0.5	0.9
	Channelized incision	411.0	−14.0 ± 1.7	−3.4
	Basin total	12,419.9	187.5 ± 52.3	1.5

* Negative values of volumetric change and average ΔZ indicate deposition.

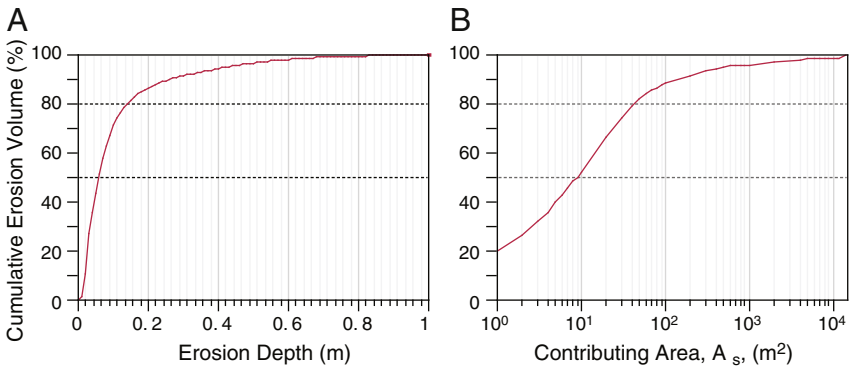

Fig. 8. Cumulative frequency distribution of volume of material by depth of erosion and contributing area.

noted that although the channel was a sink for material mobilized during our analysis period, qualitative field observations indicate it became an important source of material for subsequent debris flows recorded at the site in the months following our last scan. These later debris flows eventually scoured most of the channel to bedrock (Kean et al., 2011).

Furthermore, we speculate that the introduction of a large quantity of sediment from rilling and raveling processes produces a transport-limited environment within the channelized incision process domain during the analyzed rainstorm. The large quantities of sediment available for transport during the event permit the high sediment concentration values necessary for debris flow. Further work is needed to see if this situation is common to runoff-generated debris flows. If so, this rapid introduction of a large quantity of sediment from hillslopes may prove to be a critical process for the transition of surface flow to debris-flow during runoff-generated debris-flow events in small headwater drainage basins where there is no discrete hillslope failure. In addition, deposits not eroded and material transported within the storm and by pre- and post-storm raveling provide material for subsequent debris flows, of which there were several in the study basin later in the winter (Kean et al., 2011).

It is important to note that our results represent the topographic changes that were produced during a single rainstorm in close temporal

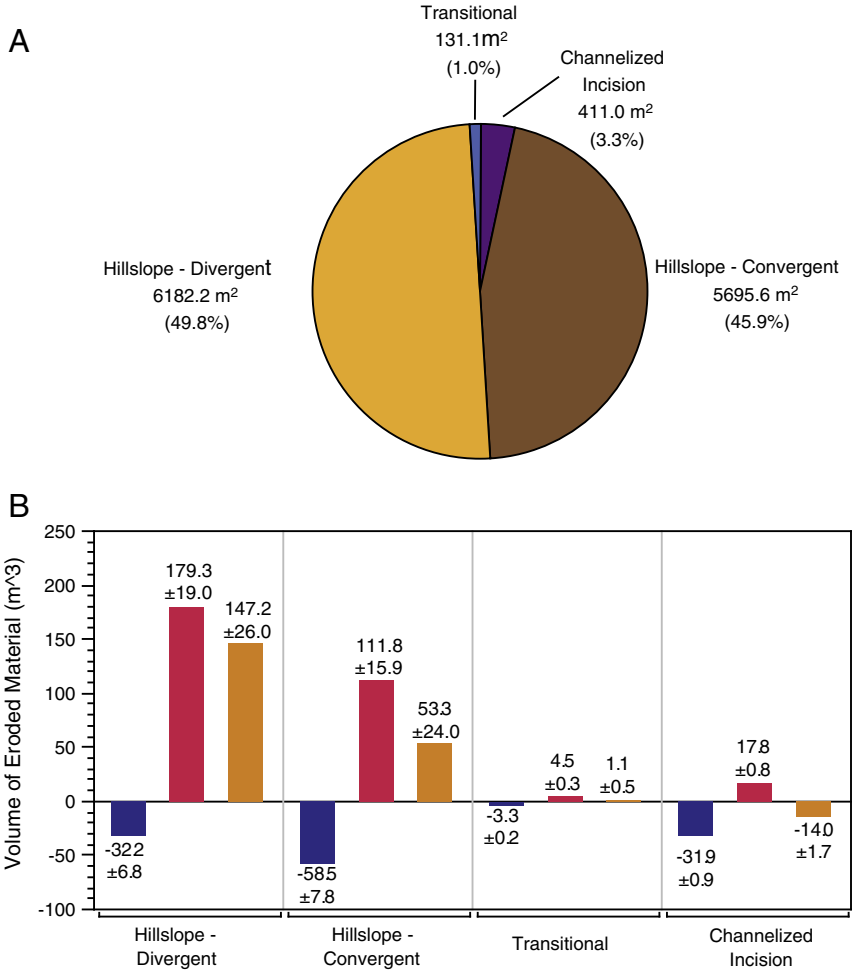

Fig. 9. Areal characteristics and sediment budget of each process domain. (A) Proportion of total basin area within each process domain; (B) summary of total volume of erosion, deposition, and net sediment yield for each process domain. Note that negative values in (B) represent deposition.

proximity (three months) to the wildfire. As the length of time and number of rainstorms since wildfire increases, sediment availability will evolve and vegetation will recover. These changes will not only reduce the amount of sediment available to transport, but will also reduce the importance of rainfall-dependent transport processes and the generation of overland flow on hillslopes. Further work is needed to characterize the relation between sediment availability, recovery of post-fire steeplands and the potential for debris-flow hazards in these areas. Continued TLS monitoring of these areas throughout the first winter after wildfire will advance our understanding of these relations.

7. Conclusions

Morphometric analyses of very high-resolution topographic data from multi-temporal TLS surveys allow for the spatial characterization of the magnitude of total erosion, total deposition and net erosion in response to a debris-flow producing rainstorm in a recently burned headwater basin. Area–slope analysis based on a 2.5 cm DEM combined with calculation of surface curvature allowed for the segregation of the basin into four morphometrically defined process domains: hillslope-divergent, hillslope-convergent, transitional, and channelized incision. This analysis revealed a critical transition between hillslope processes and channelized incision at or near the location where contributing area exceeded 100 m^2, which was verified by field mapping of geomorphic features. From these data, we determined that the hillslope-divergent process domain was the primary source of material eroded from the basin (57% of the net erosion), followed closely by the hillslope-convergent process domain (36% of the net erosion). Our results highlight the importance of erosional processes operating on hillslopes in contributing material to post-fire debris flows where there is no discrete material source or initiation point. The methods and results described here may be used to provide spatial constraints for predictive models of processes that contribute to post-fire debris-flow initiation. Furthermore, our results provide an unprecedented description of post-fire sediment budget and sediment delivery ratios that may be used to better constrain predictive models of post-fire debris-flow volume. Additional work is needed to evaluate the generality of our measurements, and assess how the results of geomorphic change detection studies derived from very high-resolution data sources (e.g., TLS) might be up-scaled for use with lower-resolution data obtained from airborne and satellite sources.

Geomorphic change detection methods using TLS data and subsequent analysis presented in this paper offer the potential to carry out cost-effective event-based analysis of topographic changes which provide insight into the geomorphic processes responsible for the short-term evolution of landscapes. Whereas we identified that the hillslopes provided the greatest amount of material for the entirety of the study, little is known of the spatial and temporal evolution of the erosional response during the rainstorm. Improved technological capabilities and innovative methods of automatically documenting the topographic changes during a debris-flow event will provide even greater improvements in our understanding of the processes responsible for the initiation and growth of debris-flows during high-intensity rainstorms in recently burned watersheds.

Acknowledgments

This work was supported by the National Geographic Society Proposal # 002929-2009-0046-1, National Science Foundation Grant Nos. 02–39749 and 09–34131 and the U.S. Geological Survey (USGS) Landslide Hazards Program. Jeff Coe (USGS), John Moody (USGS), Kerry Tompkins (CSIRO) and an anonymous reviewer provided insightful comments and suggestions which have greatly improved this manuscript. Any use of trade, product, or firm names is for descriptive purposes only and does not imply endorsement by the U.S. Government.

References

Bagheri Bodaghabadi, M., Salehi, M.H., Martínez-Casasnovas, J.A., Mohammadi, J., Toomanian, N., Esfandiarpoor Borujeni, I., 2011. Using Canonical Correspondence Analysis (CCA) to identify the most important DEM attributes for digital soil mapping applications. Catena 86, 66–74.
Bennett, G.L., Molnar, P., Eisenbeiss, H., McArdell, B.W., 2012. Erosional power in the Swiss Alps: characterization of slope failure in the Illgraben. Earth Surface Processes and Landforms 37, 1627–1640.
Beven, K.J., Kirkby, M.J., 1979. A physically based, variable contributing area model of basin hydrology. Hydrological Sciences Bulletin 24, 43–69.
Blaszczynski, J.S., 1997. Landform characterization with geographic information systems. Photogrammetric Engineering & Remote Sensing 63, 183–191.
Brasington, J., Langham, J., Rumsby, B., 2003. Methodological sensitivity of morphometric estimates of coarse fluvial sediment transport. Geomorphology 53, 299–316.
Cannon, S.H., 2001. Debris-flow generation from recently burned watersheds. Environmental and Engineering Geoscience 7, 321–341.
Cannon, S.H., DeGraff, J., 2009. The increasing wildfire and post-fire debris-flow threat in Western USA, and implications for consequences of climate change. In: Sassa, K., Canuti, P. (Eds.), Landslides — Disaster Risk Reduction. Springer, Berlin Heidelberg, pp. 177–190.
Cannon, S.H., Reneau, S.L., 2001. Conditions for generation of fire-related debris flows, Capulin Canyon, New Mexico. Earth Surface Processes and Landforms 25, 1103–1121.
Cannon, S.H., Bigio, E.R., Mine, E., 2001a. A process for fire-related debris flow initiation, Cerro Grande fire, New Mexico. Hydrological Processes 15, 3011–3023.
Cannon, S.H., Kirkham, R.M., Parise, M., 2001b. Wildfire-related debris-flow initiation processes, Storm King Mountain, Colorado. Geomorphology 39, 171–188.
Cannon, S.H., Gartner, J.E., Parrett, C., Parise, M., 2003. Wildfire-related debris-flow generation through episodic progressive sediment-bulking processes, western USA. In: Rickenmann, D., Chen, C.L. (Eds.), Debris-Flow Hazards Mitigation — Mechanics, Prediction, and Assessment. Proceedings of the Third International Conference on Debris-Flow Hazards Mitigation, Davos, Switzerland, 10–12 September 2003. A.A. Balkema, Rotterdam, pp. 71–82.
Cannon, S.H., Gartner, J.E., Wilson, R., Bowers, J., Laber, J., 2008. Storm rainfall conditions for floods and debris flows from recently burned areas in southwestern Colorado and Southern California. Geomorphology 96, 250–269.
Cannon, S., Boldt, E., Laber, J., Kean, J., Staley, D., 2011. Rainfall intensity–duration thresholds for postfire debris-flow emergency-response planning. Natural Hazards 59, 209–236.
Chawner, W.D., 1935. Alluvial fan flooding: the Montrose, California flood of 1934. Geographical Review 25, 235–263.
Costa, J.E., 1984. Physical geomorphology of debris flows. In: Costa, J.E., Fleisher, P.J. (Eds.), Developments and Applications of Geomorphology. Springer-Verlag, Berlin, pp. 268–317.
Dietrich, W.E., Wilson, C.J., Montgomery, D.R., McKean, J., Bauer, R., 1992. Erosion thresholds and land surface morphology. Geology 20, 675–679.
Dietrich, W.E., Wilson, C.J., Montgomery, D.R., McKean, J., 1993. Analysis of erosion thresholds, channel networks and landscape morphology using digital elevation models. Journal of Geology 101, 259–278.
Doehring, D.O., 1968. The effect of fire on geomorphic processes in the San Gabriel Mountains, California. Rocky Mountain Geology 7, 43–65.
Eaton, E.C., 1935. Flood and erosion control problems and their solution. Proceedings of the American Society of Civil Engineers 62, 1302–1362.
Evans, I.S., 1972. General geomorphometry, derivatives of altitude, and descriptive statics. In: Chorley, R.J. (Ed.), Spatial Analysis in Geomorphology. Harper & Row, London, pp. 17–90.
Evans, I.S., 1987. The morphometry of specific landforms. In: Gardiner, V. (Ed.), International Geomorphology 1986, vol. II. John Wiley and Sons, New York, pp. 105–124.
Florsheim, J.L., Keller, E.A., Best, D.W., 1991. Fluvial sediment transport in response to moderate storm flows following chaparral wildfire, Ventura County, Southern California. Geological Society of America Bulletin 103, 504–511.
Gabet, E.J., 2003a. Post-fire thin debris flows: sediment transport and numerical modelling. Earth Surface Processes and Landforms 28, 1341–1348.
Gabet, E.J., 2003b. Sediment transport by dry ravel. Journal of Geophysical Research 108, 2049. http://dx.doi.org/10.1029/2001JB001686 (B1).
Hamilton, E.L., Horton, J.S., Rowe, P.B., Reimann, L.F., 1954. Fire–flood sequences on the San Dimas Experimental Forest. U.S. Department of Agriculture, Forest Service, California Forest and Range Experiment, Technical Paper 6.
Hancock, G.R., Crawter, D., Fityus, S.G., Chandler, J., Wells, T., 2008. The measurement and modelling of rill erosion at angle of repose slopes in mine spoil. Earth Surface Processes and Landforms 33, 1006–1020.
Heritage, G., Hetherington, D., 2007. Towards a protocol for laser scanning in fluvial geomorphology. Earth Surface Processes and Landforms 32, 66–74.
Heritage, G.L., Milan, D.J., Large, A.R.G., Fuller, I.C., 2009. Influence of survey strategy and interpolation model on DEM quality. Geomorphology 112, 334–344.
Hurst, M.D., Mudd, S.M., Walcott, R., Attal, M., Yoo, K., 2012. Using hilltop curvature to derive the spatial distribution of erosion rates. Journal of Geophysical Research 117, F02017. http://dx.doi.org/10.1029/2011JF002057.
Ijjasz-Vasquez, E.J., Bras, R.L., 1995. Scaling regimes of local slope versus contributing area in digital elevation models. Geomorphology 12, 299–311.
Innes, J.L., 1983. Debris flows. Progress in Physical Geography 7, 469–501.
Isenburg, M., 2012. LasTools: award winning software for rapid LiDAR processing. http://rapidlasso.com/ (accessed 06 February, 2014).
Iverson, R.M., 2000. Landslide triggering by rain infiltration. Water Resources Research 36, 1897–1910.
Jaboyedoff, M., Demers, D., Locat, J., Locat, A., Locat, P., Oppikofer, T., Robitaille, D., Turmel, D., 2009. Use of terrestrial laser scanning for the characterization of retrogressive

landslides in sensitive clay and rotational landslides in river banks. Canadian Geotechnical Journal 46, 1379–1390.
Jaboyedoff, M., Oppikofer, T., Abellán, A., Derron, M.-H., Loye, A., Metzger, R., Pedrazzini, A., 2012. Use of LiDAR in landslide investigations: a review. Natural Hazards 61, 5–28.
Johnson, A.M., Rodine, J.R., 1984. Debris flow. In: Brundsen, D., Prior, D.B. (Eds.), Slope Instability. John Wiley and Sons, New York, pp. 257–361.
Kean, J.W., Staley, D.M., 2011. Direct measurements of the hydrologic conditions leading up to and during post-fire debris flow in Southern California, USA. 5th International Conference on Debris-Flow Hazards Mitigation: Mechanics, Prediction, and Assessment, Padua, pp. 685–694.
Kean, J.W., Staley, D.M., Cannon, S.H., 2011. In situ measurements of post-fire debris flows in Southern California: comparisons of the timing and magnitude of 24 debris-flow events with rainfall and soil moisture conditions. Journal of Geophysical Research: Earth Surface 116, F04019. http://dx.doi.org/10.1029/2011JF002005.
Kean, J.W., Staley, D.M., Leeper, R.J., Schmidt, K.M., 2012. A low-cost method to measure the timing of post-fire flash floods and debris flows relative to rainfall. Water Resources Research 48, W05516. http://dx.doi.org/10.1029/2011WR011460.
Kean, J.W., McCoy, S.W., Tucker, G.E., Staley, D.M., Coe, J.A., 2013. Runoff-generated debris flows: observations and modeling of surge initiation, magnitude, and frequency. Journal of Geophysical Research: Earth Surface 118, 2190–2207.
Kinnell, P.I.A., 2005. Raindrop-impact-induced erosion processes and prediction: a review. Hydrological Processes 19, 2815–2844.
Kirkby, M.J., 1971. Hillslope process-response models based on the continuity equation. Institute of British Geographers Special Publication 3, 15–30.
Lamb, M.P., Scheingross, J.S., Amidon, W.H., Swanson, E., Limaye, A., 2011. A model for fire-induced sediment yield by dry ravel in steep landscapes. Journal of Geophysical Research: Earth Surface 116, F03006. http://dx.doi.org/10.1029/2010JF001878.
Lane, S.N., Chandler, J.H., Richards, K.S., 1998. Landform monitoring, modelling and analysis: land form in geomorphological research. In: Lane, S.N., Chandler, J.H., Richards, K.S. (Eds.), Landform Monitoring, Modelling and Analysis. John Wiley and Sons Ltd., New York, pp. 1–17.
Lane, S.N., Westaway, R.M., Hicker, D.M., 2003. Estimation of erosion and deposition volume in a large gravel-bed, braided river using synoptic remote sensing. Earth Surface Processes and Landforms 28, 249–271.
Lavé, J., Burbank, D., 2004. Denudation processes and rates in the Transverse Ranges, Southern California: erosional response of a transitional landscape to external and anthropogenic forcing. Journal of Geophysical Research: Earth Surface 109, F01006. http://dx.doi.org/10.1029/2003JF000023.
May, C.L., 2007. Sediment and wood routing in steep headwater streams: an over view of geomorphic processes and their topographic signatures. Forest Science 53, 119–130.
McCoy, S.W., Kean, J.W., Coe, J.A., Staley, D.M., Wasklewicz, T.A., Tucker, G.E., 2010. Evolution of a natural debris flow: in situ measurements of flow dynamics, video imagery, and terrestrial laser scanning. Geology 38, 735–738.
McPhee, J.A., 1989. The Control of Nature. Farrar Straus and Giroux, New York.
Meyer, G.A., Wells, S.G., 1997. Fire-related sedimentation events on alluvial fans, Yellowstone National Park, U.S.A. Journal of Sedimentary Research 67, 776–791.
Milan, D.J., Heritage, G.L., Hetherington, D., 2007. Application of a 3D laser scanner in the assessment of erosion and deposition volumes and channel change in a proglacial river. Earth Surface Processes and Landforms 32, 1657–1674.
Milan, D.J., Heritage, G.L., Large, A.R.G., Fuller, I.C., 2011. Filtering spatial error from DEMs: implications for morphological change estimation. Geomorphology 125, 160–171.
Millares, A., Gulliver, Z., Polo, M.J., 2012. Scale effects on the estimation of erosion thresholds through a distributed and physically-based hydrological model. Geomorphology 153 (154), 115–126.
Minár, J., Evans, I.S., 2008. Elementary forms for land surface segmentation: the theoretical basis of terrain analysis and geomorphological mapping. Geomorphology 95, 236–259.
Montgomery, D.R., 2001. Slope distributions, threshold hillslopes, and steady-state topography. American Journal of Science 301, 432–454.
Montgomery, D.R., Dietrich, W.E., 1989. Source areas, drainage density, and channel initiation. Water Resources Research 25, 1907–1918.
Montgomery, D.R., Dietrich, W.E., 1994. Landscape dissection and drainage area–slope thresholds. In: Kirkby, M.J. (Ed.), Process Models and Theoretical Geomorphology. John Wiley and Sons Ltd., New York, pp. 221–246.
Montgomery, D.R., Foufoula-Georgiou, E., 1993. Channel network source representation using digital elevation models. Water Resources Research 29, 3925–3934.
Montgomery, D.R., Schmidt, K.M., Dietrich, W.E., McKean, J., 2009. Instrumental record of debris flow initiation during natural rainfall: implications for modeling slope stability. Journal of Geophysical Research: Earth Surface 114, F01031. http://dx.doi.org/10.1029/2008JF001078.
Moody, J.A., Kinner, D.A., 2006. Spatial structures of stream and hillslope drainage networks following gully erosion after wildfire. Earth Surface Processes and Landforms 31, 319–337.
Moody, J.A., Martin, D.A., 2009. Synthesis of sediment yields after wildland fire in different rainfall regimes in the western United States. International Journal of Wildland Fire 18, 96–115.
Nyman, P., Sheridan, G.J., Smith, H.G., Lane, P.N.J., 2011. Evidence of debris flow occurrence after wildfire in upland catchments of south-east Australia. Geomorphology 125, 383–401.
Parrett, C., 1987. Fire-related debris flows in the Beaver Creek Drainage, Lewis and Clark County, Montana. U.S. Geological Survey Water-Supply Paper 233057, pp. 57–67.
Passalacqua, P., Do Trung, T., Foufoula-Georgiou, E., Sapiro, G., Dietrich, W.E., 2010a. A geometric framework for channel network extraction from LiDAR: nonlinear diffusion and geodesic paths. Journal of Geophysical Research: Earth Surface 115, F01002. http://dx.doi.org/10.1029/2009JF001254.
Passalacqua, P., Tarolli, P., Foufoula-Georgiou, E., 2010b. Testing space-scale methodologies for automatic geomorphic feature extraction from LiDAR in a complex mountainous landscape. Water Resources Research 46, W11535. http://dx.doi.org/10.1029/2009WR008812.
Prosser, I.P., Abernethy, B., 1996. Predicting the topographic limits to a gully network using a digital terrain model and process thresholds. Water Resources Research 32, 2289–2298.
Prosser, I.P., Rustomji, P., 2000. Sediment transport capacity relations for overland flow. Progress in Physical Geography 24, 179–193.
Reneau, S.L., Dietrich, W.E., 1987. The importance of hollows in debris flow studies; examples from Marin County, CA. Debris flows/avalanches; process, recognition, and mitigation. Reviews in Engineering Geology 165–180.
Santi, P., Dewolfe, V., Higgins, J., Cannon, S., Gartner, J., 2008. Sources of debris flow material in burned areas. Geomorphology 96, 310–321.
Schmidt, K.M., Hanshaw, M.N., Howle, J.F., Kean, J.W., Staley, D.M., Stock, J.D., Bawden, G.W., 2011. In: Genevois, R., Hamilton, D.L., Prestininzi, A. (Eds.), Hydrologic conditions and terrestrial laser scanning of post-fire debris flows in the San Gabriel Mountains, CA, USA. Italian Journal of Engineering Geology and Environment — Book. Casa Editrice Universita La Sapienza, Rome, Italy, pp. 583–593.
Schumm, S.A., Lichty, R.W., 1965. Time, space and causality in geomorphology. American Journal of Science 263, 110–119.
Schurch, P., Densmore, A.L., Rosser, N.J., McArdell, B.W., 2011. Dynamic controls on erosion and deposition on debris-flow fans. Geology 39, 827–830.
Scott, K.M., 1971. Origin and sedimentology of 1969 debris flows near Glendora, California, Geological Survey Research 1971, Chapter C. U.S. Geological Survey Professional Paper 750C, C242–C247.
Shakesby, R., Doerr, S., 2006. Wildfire as a hydrological and geomorphological agent. Earth-Science Reviews 74, 269–307.
Smith, H.G., Sheridan, G.J., Nyman, P., Child, D.P., Lane, P.N.J., Hotchkis, M.A.C., Jacobsen, G.E., 2012. Quantifying sources of fine sediment supplied to post-fire debris flows using fallout radionuclide tracers. Geomorphology 139 (140), 403–415.
Staley, D.M., Wasklewicz, T.A., Blaszczynski, J.S., 2006. Surficial patterns of debris flow deposition on alluvial fans in Death Valley, CA using airborne laser swath mapping data. Geomorphology 74, 152–163.
Staley, D.M., Wasklewicz, T.A., Coe, J.A., Kean, J.W., McCoy, S.W., Tucker, G.E., 2011. Observations of debris flows at Chalk Cliffs, Colorado, USA: part 2, changes in surface morphometry from terrestrial laser scanning in the summer of 2009. In: Genevois, R., Hamilton, D.L., Prestininzi, A. (Eds.), Proceedings of the Fifth International Conference on Debris Flow Hazards Mitigation/Mechanics, Prediction, and Assessment, Padua, Italy, June 7–11, 2011. 5th International Conference on Debris-Flow Hazards Mitigation: Mechanics, Prediction, and Assessment. Italian Journal of Engineering Geology and Environment — Book. Casa Editrice Universita La Sapienza, Rome, Italy, pp. 715–724.
Staley, D.M., Kean, J.W., Cannon, S.H., Schmidt, K.M., Laber, J.L., 2013. Objective definition of rainfall intensity–duration thresholds for the initiation of post-fire debris flows in Southern California. Landslides 10, 547–562.
Stefano, C.D., Ferro, V., Porto, P., Tusa, G., 2000. Slope curvature influence on soil erosion and deposition processes. Water Resources Research 36, 607–617.
Stock, J., Dietrich, W.E., 2003. Valley incision by debris flows: evidence of a topographic signature. Water Resources Research 39, 1089. http://dx.doi.org/10.1029/2001WR001057 (4).
Stock, J.D., Dietrich, W.E., 2006. Erosion of steepland valleys by debris flows. Geological Society of America Bulletin 118, 1125–1148.
Tarboton, D.G., 1997. A new method for the determination of flow directions and upslope areas in grid digital elevation models. Water Resources Research 33, 309–319.
Tarboton, D.G., Bras, R.L., Rodriguez-Iturbe, I., 1992. A physical basis for drainage density. Geomorphology 5, 59–76.
Taylor, J.R., 1982. Introduction to Error Analysis: The Study of Uncertainty in Physical Measurements. University Science Books, Mill Valley, CA.
Tucker, G.E., Lancaster, S.T., Gasparini, N.M., Bras, R.L., 2001. The channel–hillslope integrated landscape development model. In: Harmon, R.S., Doe, W.W. (Eds.), Landscape Erosion and Evolution Modeling. Kluwer Press, Dordrecht, pp. 349–388.
Wester, T., Wasklewicz, T., Staley, D., 2014. Functional and structural connectivity within a recently burned drainage basin. Geomorphology 206, 362–373.
Wheaton, J.M., Brasington, J., Darby, S.E., Sear, D.A., 2010. Accounting for uncertainty in DEMs from repeat topographic surveys: improved sediment budgets. Earth Surface Processes and Landforms 35, 136–156.
Willgoose, G., 1994. A physical explanation for an observed area–slope–elevation relationship for catchments with declining relief. Water Resources Research 30, 151–159.
Willgoose, G., Bras, R.L., Rodriguez-Iturbe, I., 1991. A physical explanation of an observed link area–slope relationship. Water Resources Research 27, 1697–1702.
Yerkes, R.F., Cambell, R.H., 2005. Preliminary geologic map of the Los Angeles 30′ × 60′ Quadrangle, Southern California. U.S. Geological Survey Open File Report 2005–1019.
Zevenbergen, L.W., Thorne, C.R., 1987. Quantitative analysis of land surface topography. Earth Surface Processes and Landforms 12, 47–56.